



3 Seismology and Earth Structure

Ordinary language undergoes modification to a high pressure form when applied to the interior of the earth; a few examples of equivalents follow:

Ordinary meaning:

*dubious
perhaps
vague suggestion
trivial objection
uncertain mixture of all the elements*

High pressure form:

*certain
undoubtedly
positive proof
unanswerable argument
pure iron*

Francis Birch, 1952

3.1 Introduction

A major application of seismology is the determination of the distribution of seismic velocities, and hence elastic properties, within the earth. This distribution, known as *earth structure*, gives the basic constraint on the mineralogical, chemical, and thermal state of the earth's interior. Seismological data are important for this purpose because their resolving power is generally superior to that of other geophysical methods. For example, although gravity and magnetic data indicate the presence of a dense fluid core at depth, they provide only relatively weak constraints on its density and size. By contrast, seismological data indicate the depth of the core–mantle boundary and the sharp change in properties that occurs there. Above the boundary, both *P* and *S* waves propagate in the solid mantle, whereas in the liquid outer core no *S* waves propagate and the *P*-wave velocity drops sharply. The observed velocities are the primary basis for our models of the physical properties and chemical composition of the material on either side of this boundary. Similarly, the distinction between the crust and the mantle and many inferences about their structure and composition come from seismological observations. More generally, by establishing the essentially layered structure of the earth, seismology provides the primary evidence for the process of differentiation whereby material within planets became compositionally segregated during their evolution. As a result, many crucial issues about the other terrestrial planets could be resolved if seismological data were available.

Constraints from seismology are crucial for other disciplines of the earth sciences, and vice versa. Seismology gives *earth models* describing the distribution of *P*- and *S*-wave velocities and density. Going from an earth model to a description of the chemical, mineralogical, thermal, and rheological state of the earth's interior requires additional information. There are thus two types of uncertainty in our knowledge of the earth's interior. In some cases, such as the structure of the inner core, the seismological results are still under discussion. In others—for example, the nature of the 660 km discontinuity in the mantle—the basic seismological results are generally accepted, but their mineralogic and petrologic interpretations remain under investigation. Given our scope here, we only summarize the implications of seismological data for models of the earth's interior.

The fundamental data for seismological studies of the earth's interior are the travel times of seismic waves. The measurements available are the arrival times of seismic waves at receivers. To convert these to travel times, the origin time and location of the source must be known. These parameters, which are known for artificial sources, must be estimated from the observations for earthquake sources. Hence travel time data include information about both the source and the properties of the medium, and separating the two is a challenge in many seismological studies.

The travel times are used to learn about the velocity structure between the source and the receiver. As we saw in the last chapter, waves follow paths that depend on the velocity

structure. Hence the structure must be known to find the paths that the waves took. To illustrate this, consider the travel time between two points. If the velocity were constant, the ray path would be a straight line, and the velocity could be found by dividing the distance by the travel time. If, instead, an interface separates media with different velocities, the ray path would consist of two line segments, depending on the velocities, and the travel time would be the sum of the time spent along each segment. For a more complicated velocity distribution, the ray path would also be more complicated.

This problem can be posed mathematically by writing the travel time between the source (s) and receiver (r) as the integral of 1/velocity, or slowness, along the ray path

$$T(s, r) = \int_s^r \frac{1}{v(x)} dx. \quad (1)$$

In simple cases, where the ray path is a set of segments with constant velocity, the integral is just a sum over the time in each segment. Thus the travel time gives an integral constraint on the velocity distribution between the source and the receiver, but does not indicate which of the many paths satisfying the constraint the ray followed. As a result, an individual measurement is inadequate to show the distribution of velocities. Fortunately, as we shall see, a set of travel times between different sources and receivers provides much more information. In addition, useful information is derived from the amplitudes and waveforms of seismic waves.

This example illustrates an interesting feature of determining velocity structure from travel times. If the velocity structure is known, the forward problem of finding the travel times and amplitudes is straightforward. However, the inverse problem of using the travel times and amplitudes measured at the surface to find the velocity structure at depth is more difficult, and various methods are used. For example, in addition to using travel times directly, we have seen that velocity structure is studied using the dispersion of surface waves (Section 2.8) and the eigenfrequencies of normal modes (Section 2.9), quantities that correspond to travel times.

In this chapter, we follow the approach discussed in Section 1.1.2 of treating the earth with a series of progressively more complex and, hopefully, more accurate models. We begin with the homogeneous, isotropic, elastic, layered halfspace used in Chapter 2 to derive seismic wave propagation. This approximation of uniform flat layers is often used in crust and upper mantle studies, where the distance between source and receiver is less than a few hundred kilometers. We then consider larger source-receiver distances, for which spherical geometry is required, and then the anisotropic and anelastic behavior of the earth. Throughout these discussions, we will see that although velocity varies primarily with depth, there are important lateral variations, or heterogeneities. Finally, we consider the implications of the observed heterogeneous, anisotropic, and anelastic

velocity structure for the composition of the earth. Later, in Chapter 7, we discuss further how seismic data can be used to study laterally variable velocity structure.

3.2 Refraction seismology

3.2.1 Flat layer method

The simplest approach to the inverse problem of determining velocity at depth from travel times treats the earth as flat layers of uniform-velocity material. We thus begin by deriving the travel time curves for such a model, which show when seismic waves arrive at a particular distance from a seismic source. The travel times, especially those of waves that are critically refracted at the interfaces, are used to find the velocities of the layers and underlying halfspace and the layer thicknesses. As a result, this technique is called *refraction seismology*.

Refraction seismology is used on vastly differing scales. Near-surface structure at depths less than 100 meters can be studied using a sledge hammer or a shotgun as a source and a single receiver. Similar methods are used to study the crust and the upper mantle, with earthquake or explosion sources and many receivers at distances of hundreds of kilometers.

The simplest situation, shown in Fig. 3.2-1, is a layer of thickness h_0 , with velocity v_0 , overlying a halfspace with a higher velocity, v_1 . We write the velocities as “ v ” to indicate that the analysis applies for either P or S waves. There are three basic ray paths from a source on the surface at the origin to a surface receiver at x . The travel times for these paths can be found using Snell’s law.

The first ray path corresponds to a *direct wave* that travels through the layer with travel time

$$T_D(x) = x/v_0. \quad (1)$$

This travel time curve (Fig. 3.2-2) is a linear function of distance, with slope $1/v_0$, that goes through the origin.

The second ray path is for a wave reflected from the interface. Because the angles of incidence and reflection are equal,

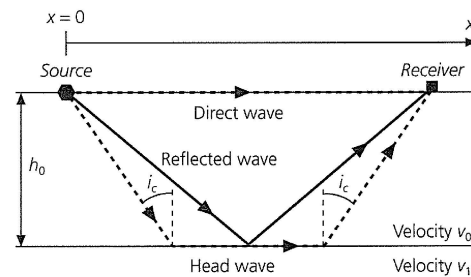


Fig. 3.2-1 Three basic ray paths for a layer over a halfspace model. The direct and reflected rays travel within the layer, whereas the head wave path also includes a segment just below the interface. For the head wave to exist, the layer velocity v_0 must be less than the halfspace velocity v_1 .

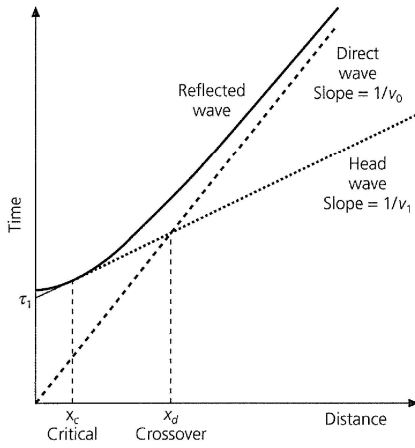


Fig. 3.2-2 Travel time versus source-to-receiver distance plot for the three ray paths in Fig. 3.2-1. The direct wave is the first arrival for receivers closer than the crossover distance x_d . Beyond x_d the head wave arrives first. The head wave exists only beyond the critical distance x_c .

the wave reflects halfway between the source and the receiver. The travel time curve can be found by noting that $x/2$ and h_0 form two sides of a right triangle, so

$$T_R(x) = 2(x^2/4 + h_0^2)^{1/2}/v_0. \quad (2)$$

This curve is a hyperbola, because it can be written

$$T_R^2(x) = x^2/v_0^2 + 4h_0^2/v_0^2. \quad (3)$$

For $x = 0$ the reflected wave goes straight up and down, with a travel time of $T_R(0) = 2h_0/v_0$. At distances much greater than the layer thickness ($x \gg h$), the travel time for the reflected wave asymptotically approaches that of the direct wave.

The third type of wave is the *head wave*, often referred to as a refracted wave. This wave results when a downgoing wave impinges on the interface at an angle at or beyond the critical angle. Its travel time can be computed by assuming that the wave travels down to the interface such that it impinges at the critical angle, then travels just below the interface with the velocity of the lower medium, and finally leaves the interface at the critical angle and travels upward to the surface. Thus the travel time is the horizontal distance traveled in the halfspace divided by v_1 plus that along the upgoing and downgoing legs divided by v_0 :

$$\begin{aligned} T_H(x) &= \frac{x - 2h_0 \tan i_c}{v_1} + \frac{2h_0}{v_0 \cos i_c} \\ &= \frac{x}{v_1} + 2h_0 \left(\frac{1}{v_0 \cos i_c} - \frac{\tan i_c}{v_1} \right). \end{aligned} \quad (4)$$

The last step used the fact that the critical angle (Section 2.5.5) satisfies

$$\sin i_c = v_0/v_1. \quad (5)$$

To simplify Eqn 4, we use trigonometric identities showing that

$$\cos i_c = (1 - \sin^2 i_c)^{1/2} = (1 - v_0^2/v_1^2)^{1/2} \quad (6)$$

and

$$\tan i_c = \frac{\sin i_c}{\cos i_c} = \frac{v_0/v_1}{(1 - v_0^2/v_1^2)^{1/2}}, \quad (7)$$

so Eqn 4 can be written

$$T_H(x) = x/v_1 + 2h_0(1/v_0^2 - 1/v_1^2)^{1/2} = x/v_1 + \tau_1. \quad (8)$$

Thus the head wave's travel time curve is a line with a slope of $1/v_1$ and a time axis intercept of

$$\tau_1 = 2h_0(1/v_0^2 - 1/v_1^2)^{1/2}. \quad (9)$$

This intercept is found by projecting the travel time curve back to $x = 0$, although the head wave appears only beyond the *critical distance*, $x_c = 2h_0 \tan i_c$, where critical incidence first occurs.

Because $1/v_0 > 1/v_1$, the direct wave's travel time curve has a higher slope but starts at the origin, whereas the head wave has a lower slope but a nonzero intercept. At the critical distance the direct wave arrives before the head wave. At some point, however, the travel time curves cross, and beyond this point the head wave is the first arrival even though it traveled a longer path. The *crossover distance* where this occurs, x_d , is found by setting $T_D(x) = T_H(x)$, which yields

$$x_d = 2h_0 \left(\frac{v_1 + v_0}{v_1 - v_0} \right)^{1/2}. \quad (10)$$

Hence the crossover distance depends on the velocities of the layer and the halfspace and the thickness of the layer.¹

Thus we can solve the inverse problem of finding the velocity structure at depth from the variation of the travel times observed at the surface as a function of source-receiver distance. This simple structure is described by three parameters. The two velocities, v_0 and v_1 , are found from the slope of the two travel time curves. We then identify the crossover distance and use Eqn 10 to find the third parameter, the layer thickness, h_0 . Alternatively, the layer thickness can be found from the reflection time or the head wave intercept (Eqn 9) at zero distance. Each of these methods exploits the fact that there is more than one ray path between the source and the receiver.

¹ A simple analogy is driving to a distant point by a route combining streets and a highway. If the destination is far enough away, it is quicker to take a longer route including the faster highway than a direct route on slower streets. The point at which this occurs depends on the relative speeds and the additional distance required to use the highway.

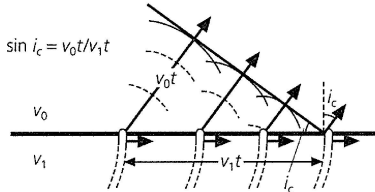


Fig. 3.2-3 Generation of an upgoing head wave by Huygens' sources due to a refracted pulse propagating along a boundary. The head wave travels in the upper layer at a slower velocity (v_0) than the refracted wave creating it, which travels in the layer below at velocity v_1 . (After Griffiths and King, 1981.)

Despite this solution's elegance, the basic assumption about the travel time of the head wave may seem unsatisfying, because it is unclear why energy should follow this path. However, the result conforms with observations — the experiment diagrammed in Fig. 3.2-1 yields an arrival whose travel time is given by Eqn 8. To understand why, we can view the head wave in several ways. As shown in this chapter's problems, it corresponds to a minimum time path between the source and the receiver, so, by Fermat's principle (Section 2.5.9), we expect such a wave. Another approach, using Huygens' principle (Section 2.5.10), is to consider the refracted wave traveling horizontally below the boundary at the velocity of the half-space, generating spherical waves that propagate upward in the lower-velocity layer (Fig. 3.2-3). The spherical waves interfere to produce upgoing plane waves that leave the interface at the critical angle.² However, our analysis of postcritical incidence (Section 2.6.4), which showed that an evanescent wave propagates along the interface, does not fully describe the head wave. A more sophisticated analysis than is appropriate here shows that the geometry in Fig. 3.2-1 gives the head wave's travel time, but not its amplitude, because geometrical optics are not applicable. Thus, although the energy propagation is more complicated than along the geometric ray path, the travel time predicted is correct.

Seismic refraction data led A. Mohorovičić³ in 1909 to one of the most important discoveries about earth structure. Observing two P arrivals (Fig. 3.2-4), he identified the first as having traveled in a deep high-velocity (7.7 km/s) layer, and the second as a direct wave in a slower (5.6 km/s) shallow layer about 50 km thick. These layers, now identified around the world, are known as the *crust* and the *mantle*. The boundary between them is known as the Mohorovičić discontinuity, or *Moho*. We now denote the head wave as P_n and the direct wave as P_g ("g" for "granitic"). Corresponding arrivals are also observed for S waves. The *Moho*, which defines the boundary

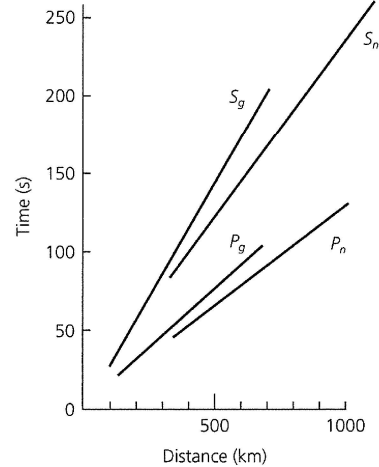


Fig. 3.2-4 Schematic of Mohorovičić's results showing the existence of a distinct crust and mantle. The travel time curves are labeled using modern nomenclature: the direct waves are P_g and S_g , and the head waves are P_n and S_n . (After Bonini and Bonini, 1979. *Eos*, 60, 699–701, copyright by the American Geophysical Union.)

between the crust and the mantle, has been observed around the world. One of the first steps in studying the nature of the crust is characterizing the depth to Moho, or crustal thickness, and the variation in P_n velocity from site to site.

Travel time plots for refraction experiments can be made by displaying seismograms in *record sections*. Because seismograms are functions of time, aligning several as a function of distance yields a travel time plot showing the different arrivals. Figure 3.2-5 shows a record section of a profile of seismograms recorded in England from explosive sources. In addition to P_n and P_g , the reflection off the Moho, known as P_mP , is well recorded. As expected, the direct and head wave travel times are linear with distance, whereas the reflection has a hyperbolic curvature. The figure is plotted as a *reduced travel time plot*, in which the time shown is the true time minus the distance divided by a constant velocity. This reduces the size of the plot, and makes waves arriving at the reducing velocity appear as a line parallel to the distance axis.

The geometry discussed here can correspond to different physical experiments. A single source can be recorded simultaneously at receivers at different distances. Alternatively, multiple sources at different distances can be recorded by a single receiver at different times. A single receiver can be moved away from a fixed source, so the same source is recorded at different distances. Similarly, a source can be moved away from a fixed receiver. Results of various experiments can be combined, using the principle of *reciprocity*, which states that the travel time is unchanged if the source and the receiver are interchanged. As a result, we can use travel time measurements without considering whether the source was at one position and the receiver at another, or the reverse. Moreover, because earth structure presumably is not changing during the experiment, data collected at different times can be combined.

² This situation is analogous to a bow wave from a boat or a supersonic wave from a jet airplane, in that the energy source travels faster than the wave it produces.

³ Andrija Mohorovičić (1857–1936), working in Zagreb, Croatia (then part of the Austro-Hungarian Empire), studied travel times from earthquakes in the region using recently invented pendulum seismographs.

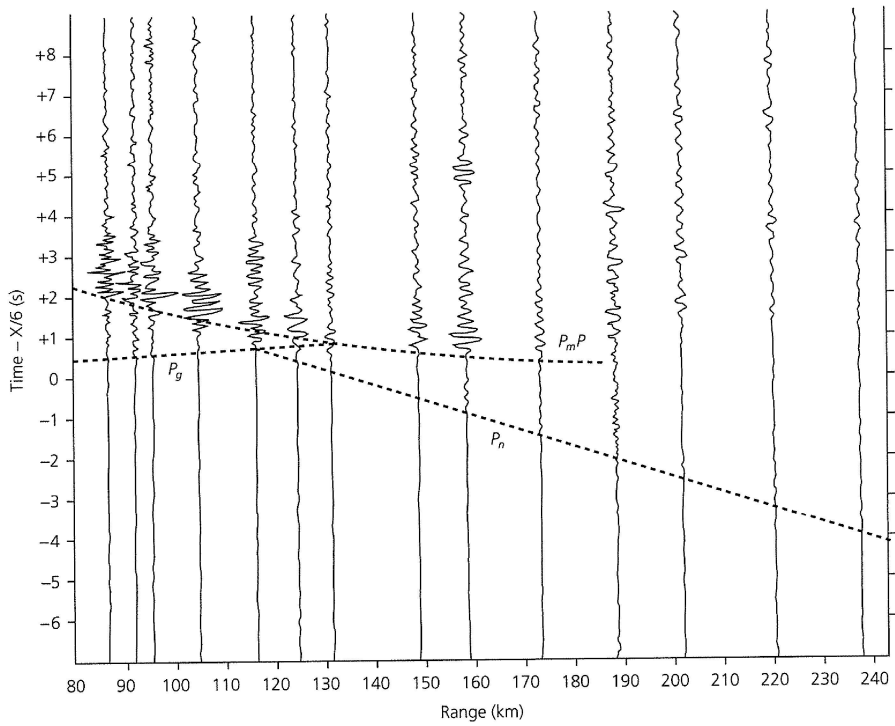


Fig. 3.2-5 Seismograms from a refraction profile, plotted with a reducing velocity of 6 km/s. The direct wave P_g , Moho head wave P_n , and Moho reflection P_mP are observed. P_n does not asymptotically approach P_mP as in Fig. 3.2-2 because the crust, instead of being homogeneous, has increasing velocity with depth. (Bott *et al.*, 1970. From *Mechanism of Igneous Intrusion*, ed. G. Newall and N. Rast, © 1970 by John Wiley & Sons Ltd. Reproduced by permission.)

Refraction data often show other arrivals in addition to P_g , P_n , and P_mP . Figure 3.2-6 shows a record section that also contains head waves P_i and P_{i2} from boundaries within the crust and the mantle and P_iP , a reflection off a mid-crustal interface, which is analogous to the P_mP reflection off the Moho.

Such data require a model with multiple layers. Figure 3.2-7 shows a model in which a head wave arises at each interface where the velocity increases with depth. The travel time curve for a head wave at the top of the n^{th} layer is a line with slope $1/v_n$, that can be extrapolated to its intercept on the t axis, τ_n , and written

$$T_{H_n}(x) = x/v_n + \tau_n, \quad (11)$$

where, by analogy to the layer over the halfspace case (Eqn 9),

$$\tau_n = 2 \sum_{j=0}^{n-1} h_j (1/v_j^2 - 1/v_n^2)^{1/2}. \quad (12)$$

The thickness of successive layers can be found by starting with the top layer, whose thickness h_0 is given by Eqn 9 or 10, and continuing downward using the iterative formula

$$h_{n-1} = \frac{\tau_n - 2 \sum_{j=0}^{n-2} h_j (1/v_j^2 - 1/v_n^2)^{1/2}}{2(1/v_{n-1}^2 - 1/v_n^2)^{1/2}}. \quad (13)$$

Thus for two layers over a halfspace, the thickness of the second layer is found by setting $n=2$, so

$$h_1 = \frac{\tau_2 - 2h_0(1/v_0^2 - 1/v_2^2)^{1/2}}{2(1/v_1^2 - 1/v_2^2)^{1/2}}. \quad (14)$$

A few examples illustrate some other complexities of refraction experiments. If the velocity increases with depth, the travel time curve for the head wave at the top of each successive layer has a shallower slope. By contrast, a low-velocity layer (Fig. 3.2-8) does not cause a head wave, so the travel time curve does not have a first arrival with the corresponding velocity, and depths to interfaces calculated using Eqn 13 are incorrect. Another possible problem occurs if a layer is thin or has a small velocity contrast with the one below it. Although a head wave results, it may never appear as a first arrival (Fig. 3.2-9), causing a *blind zone* that can be missed in the interpretation.

3.2.2 Dipping layer method

The refraction method can also be applied if the interfaces between layers are not horizontal. Conducting a *reversed profile* yields the travel times for ray paths in both the down-dip and the up-dip directions. This can be done using receivers on either side of a source, sources on either side of a receiver, or both. In this geometry, the depths to the interface below the source and the receiver differ due to the dip angle, θ . Consider

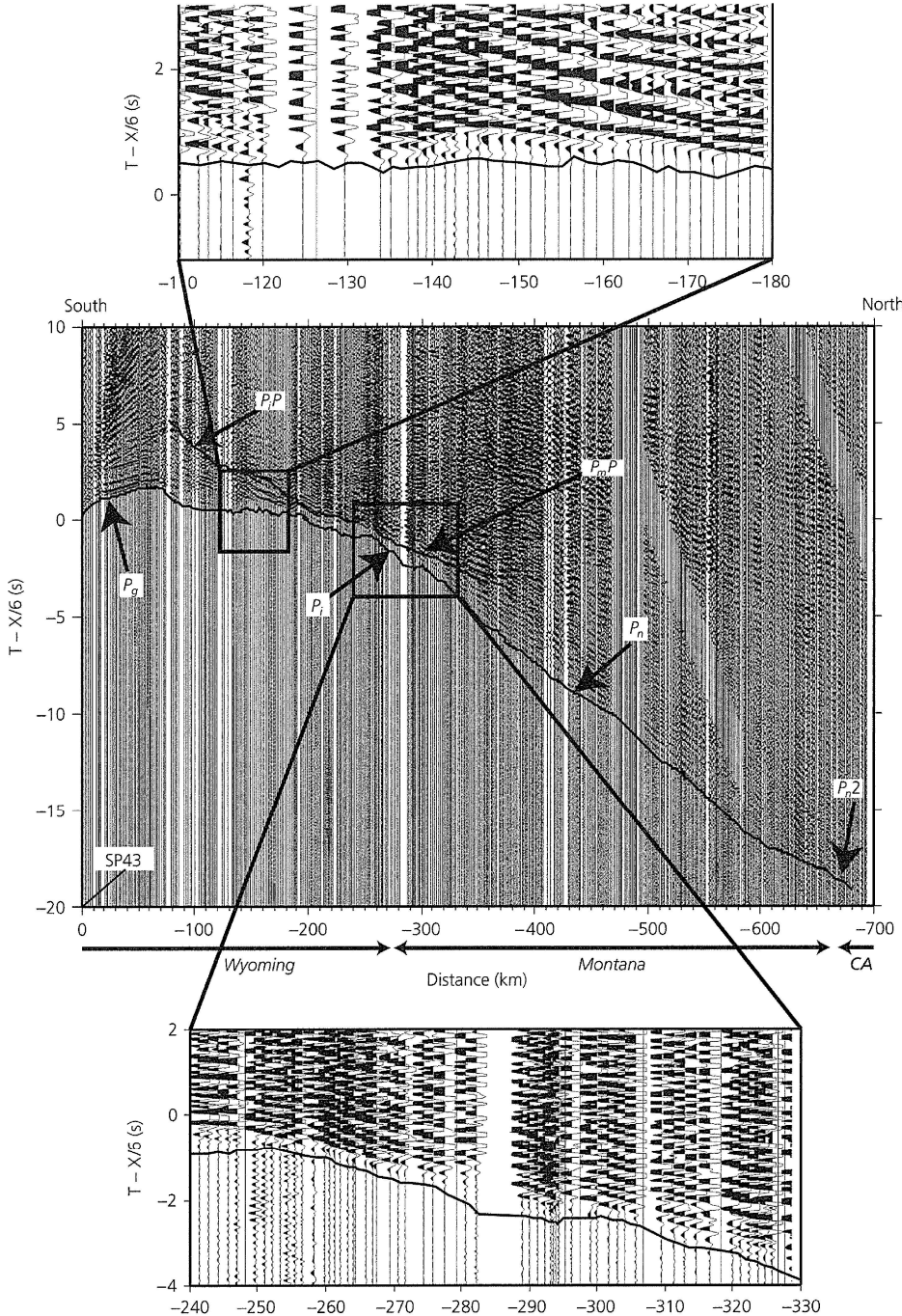


Fig. 3.2-6 Seismic refraction record section, plotted with a reducing velocity of 6 km/s. In addition to P_g , P_n , and P_mP , there are also arrivals P_i and P_{n2} interpreted as head waves from boundaries within the crust and the mantle, and P_iP , interpreted as a reflection off a mid-crustal interface. (Snelson *et al.*, 1998.)

the down-dip ray path (Fig. 3.2-10) from a source, below which the perpendicular distance to the interface is h_d , to a receiver at a distance x , below which the perpendicular distance to the interface is $(h_d + x \sin \theta)$. The travel time for the head wave in the down-dip direction is the sum of the distance

along the interface divided by v_1 plus that for the upgoing and downgoing legs divided by v_0

$$T_d(x) = \frac{x \cos \theta - (2h_d + x \sin \theta) \tan i_c}{v_1} + \frac{(2h_d + x \sin \theta)}{v_0 \cos i_c}. \quad (15)$$

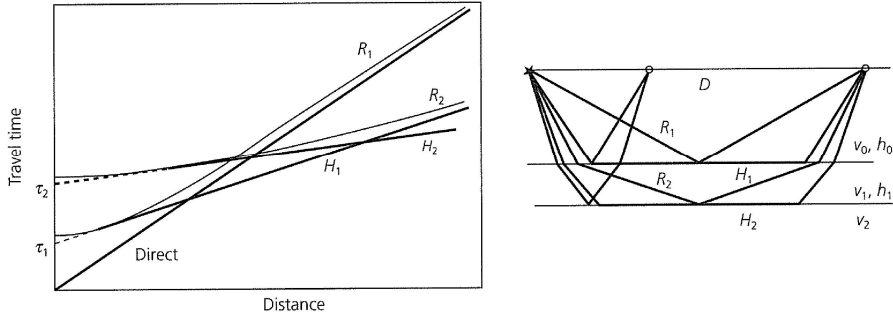


Fig. 3.2-7 Ray paths and travel times for a multilayered model in which velocity increases with depth. Each layer gives rise to a head wave H_p , whose intercept on the time axis is τ_p and a reflection R_i . The direct wave arrival is also shown.

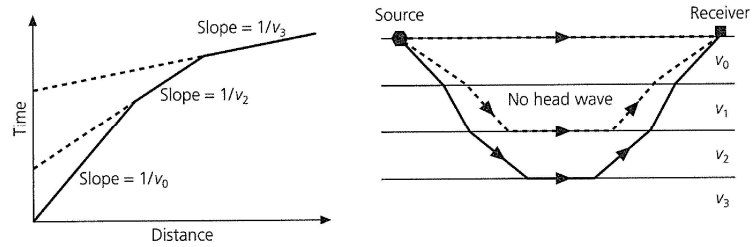


Fig. 3.2-8 Travel time curves, showing first arrivals only, for a model with three layers over a halfspace. Because the middle layer is a low-velocity layer with $v_1 < v_0$, no head wave arises at its top.

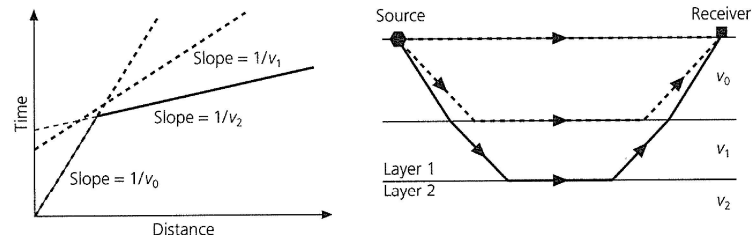
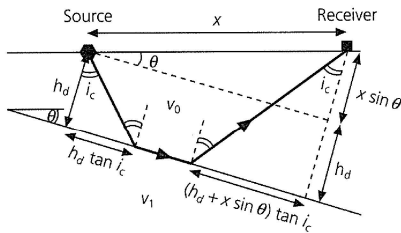


Fig. 3.2-9 Travel time curves, showing first arrivals only, for a blind zone geometry where the head wave from the top of layer 1 is never the first arrival because this layer is too thin.



For the flat case, ($\theta = 0$), this is just Eqn 4. Simplifying using Eqns 5 and 7 yields

$$\begin{aligned} T_d(x) &= \frac{x \cos \theta \sin i_c}{v_0} + \frac{(2h_d + x \sin \theta)(1 - \sin^2 i_c)}{v_0 \cos i_c} \\ &= \frac{x \sin(i_c + \theta)}{v_0} + \frac{2h_d \cos i_c}{v_0} = \frac{x}{v_d} + \tau_d, \end{aligned} \quad (16)$$

which is a straight line with slope $1/v_d$ and intercept τ_d .

Similarly, the travel time for the head wave in the up-dip direction is

$$T_u(x) = \frac{x \sin(i_c - \theta)}{v_0} + \frac{2h_u \cos i_c}{v_0} = \frac{x}{v_u} + \tau_u, \quad (17)$$

where h_u is the perpendicular distance to the interface below the receiver. Thus the apparent velocities, corresponding to the slopes of the head wave travel time curves, differ in the up-dip and down-dip directions by a factor depending on the dip angle,

$$v_u = v_0 / \sin(i_c - \theta) \quad v_d = v_0 / \sin(i_c + \theta). \quad (18)$$

The apparent velocity in the up-dip direction is greater than the halfspace velocity, and that in the down-dip direction is smaller. The time axis intercepts

$$\tau_u = 2h_u \cos i_c / v_0, \quad \tau_d = 2h_d \cos i_c / v_0, \quad (19)$$

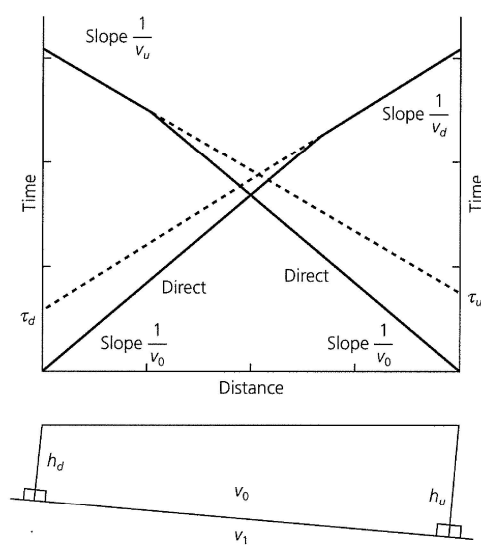


Fig. 3.2-11 Travel time plot for a reversed profile and its interpretation. The up-dip and down-dip slopes and intercepts differ.

also differ. The direct wave travel time is the same in both directions, so the crossover distances differ.

The results of a reversed profile are often displayed in the form shown in Fig. 3.2-11. The time axis is common to both directions, but distance is measured from one end of the axis for the up-dip experiment and from the other for the down-dip. The slopes of the direct and head wave travel times yield the dip angle

$$\theta = \frac{1}{2} \left(\sin^{-1} \frac{v_0}{v_d} - \sin^{-1} \frac{v_0}{v_u} \right) \quad (20)$$

and the critical angle

$$i_c = \frac{1}{2} \left(\sin^{-1} \frac{v_0}{v_d} + \sin^{-1} \frac{v_0}{v_u} \right). \quad (21)$$

The halfspace velocity v_1 is found from the critical angle and v_0 , and the intercept times then yield the layer thickness.

Two additional points about reversed profiles are worth noting. First, the different up-dip and down-dip head wave travel time curves do not imply that for a given pair of locations, it makes a difference whether the source is up-dip and the receiver down-dip, or the reverse (Fig. 3.2-12). By reciprocity, the two experiments give the same travel time. Thus, for a ray path connecting two points, it does not matter whether the wave travels up-dip or down-dip. By contrast, for two receivers at the same distance from a source, one up-dip and one down-dip, the travel times differ because the ray paths encounter the dipping interface at different depths. Similarly, the travel times

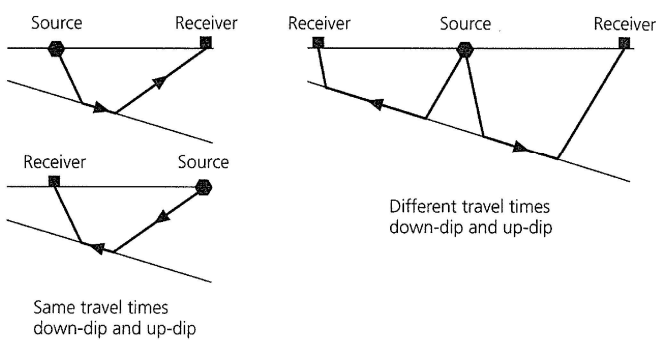


Fig. 3.2-12 Left: If the source and the receiver are interchanged on a reversed refraction profile, the travel time is unchanged. Right: Different up-dip and down-dip travel times occur because, for a given source position, waves going the same distance along the surface in opposite directions sample the dipping interface differently.

differ for two sources at the same distance from a receiver, one up-dip and one down-dip. If the dip were zero, then the travel times would be the same for all these cases because all ray paths encounter the interface at the same depth. Another way to view this is that for a flat geometry the travel time depends only on the distance between the source and the receiver. For a dipping geometry, the position as well as the separation matters, because the depth to the interface varies.

Second, the dip found from a reversed profile is not a true dip if the profile is not perpendicular to the strike of the layer. Instead, the measured dip is an apparent dip along the profile. The true dip can be found from the apparent dips along two reversed profiles that cross at a reasonably large angle, using a standard technique in structural geology.

3.2.3 Advanced analysis methods

Because the analysis above has been for simple geometries and uniform-velocity layers, refraction seismology might seem of little use in understanding the real earth. Fortunately, this is not the case. The simple geometries give models that fit data reasonably well and provide starting models for more sophisticated analyses.

Data from experiments showing travel times more complex than predicted by simple geometries can be interpreted with a computer program to trace rays using Snell's law through possible velocity structures. The predicted travel time curve is found by taking rays that arrive at a given distance, and integrating the slowness along their paths (Eqn 3.1.1). Figure 3.2-13 shows a record section and the inferred velocity structure for a refraction survey in central California. Ray paths calculated through the structure shown yield a good fit to the complicated travel time data. For example, the late arrivals about 8 km from the source are interpreted as resulting from a low-velocity region associated with a set of faults. The model